2016-01-0317
Published 04/05/2016

doi:10.4271/2016-01-0317
saealtpow.saejournals.org

Control Strategies for Power Quantized Solid Oxide Fuel Cell Hybrid Powertrains: In Mobile Robot Applications

Yuanzhan Wang, Jason B. Siegel, and Anna G. Stefanopoulou
University of Michigan

ABSTRACT

This paper addresses scheduling of quantized power levels (including part load operation and startup/shutdown periods) for a propane powered solid oxide fuel cell (SOFC) hybridized with a lithium-ion battery for a tracked mobile robot. The military requires silent operation and long duration missions, which cannot be met by batteries alone due to low energy density or with combustion engines due to noise. To meet this need we consider an SOFC operated at a few discrete power levels where maximum system efficiency can be achieved. The fuel efficiency decreases during transients and resulting thermal gradients lead to stress and degradation of the stack; therefore switching power levels should be minimized. Excess generated energy is used to charge the battery, but when it's fully charged the SOFC should be turned off to conserve fuel. However, startup and shutdown phases consume both battery and fuel energy and induce stack degradation, and therefore should be scheduled as infrequently as possible. Simple models of the battery and SOFC are used to evaluate the optimal scheduling strategy using Dynamic Programming. Representative cycles are generated from random sampling of measured power data for specific tasks. Finally a rule-based control strategy is developed and compared with the optimal one, considering battery degradation, fuel efficiency as well as design robustness. The application to military tracked robots for surveillance is considered as an example using power profiles from an instrumented PackBot; however the methodology can be applied broadly to hybrid power systems for transportation which have large turn on/off penalties.

CITATION: Wang, Y., Siegel, J., and Stefanopoulou, A., "Control Strategies for Power Quantized Solid Oxide Fuel Cell Hybrid Powertrains: In Mobile Robot Applications," *SAE Int. J. Alt. Power.* 5(1):2016, doi:10.4271/2016-01-0317.

INTRODUCTION

Currently almost all robotic vehicles are powered by Li-ion batteries. However, increasingly demanding mission duration requirements are unlikely to be met with batteries alone due to their limited energy density (190 Wh/Kg, 306 Wh/L), and there arises a need for alternative energy storage. Fuel cells are an ideal choice for augmenting battery storage, as they are more efficient than combustion engines and operate silently.

A hybrid power system combining batteries with a small propanefueled solid oxide fuel cell (SOFC) for a mobile robot has been simulated using an Ultra Electronics AMI 200 Watt fuel cell and a high energy BB2590 battery pack [1]. The SOFC power plant has a quantized on/off behavior characterized by the following properties (1) the fuel cell lacks load-following ability [1] and therefore operates most of the time at a constant power output; (2) each SOFC startup and shutdown event takes several minutes and consumes significant battery power 6.5/5.3 Wh respectively. This SOFC achieves optimum fuel utilization at full load, since the fuel flow rate is constant, and part loading is very inefficient. Therefore it is preferred to operate the FC stack in an on/off manner, however determining when to turn on and off the fuel cell to optimize fuel utilization is not trivial. While the conventional continuously operated hybrid systems [4]-[7] have been heavily studied, the quantized FC-battery hybrid has not been studied except the hybridization with a gas turbine [11]-[12]. New systematic methodologies are needed to get optimum power and endurance from this system.

This paper addresses the power split of an energy dense solid oxide fuel cell power source, hybridized with a lithium ion battery pack. The resulting power splits are tested with cycles generated from random sampling of measured power data from a PackBot while performing specific tasks [2]. Fuel cell sizing, dynamic performance (ability to change loads), and efficiency (as a function of output power) have a large impact on the performance and fuel economy of the overall system. The power split and scheduling of shutdowns are investigated via optimization (minimization of fuel consumption) using Dynamic Programming (DP) and a simulation model of hybridized battery and fuel cell system.

ENERGY REQUIREMENTS

The iRobot PackBot, which is a tracked robot, is considered for this study. The PackBot weighs 11kg without batteries or manipulator arm and is typically powered by 2 BB-2590/U lithium ion battery packs which provide more than 4 hours of continuous runtime and up to 16 kilometers of travel according to the manufacturer. Our goal is to extend the operating time beyond 10 hours, which would require 1130 Wh of energy or roughly 3x the number of batteries.

Table 1. Sample Profile Statistics

Sample Profile	Mean (W)	Standard deviation (W)	Max (W)
Pea gravel	110.7	27.0	159.5
Sand	108.7	35.9	166.4
Crushed concrete	124.7	35.0	170.7
Hill climb and decent	88.0	66.2	236.3
Obstacle	155.8	44.5	240.1
Manipulator	90.2	29.2	151.0
Synthetic	97.8	46.3	240.1

Overall hybrid system fuel efficiency (FE) will be evaluated using load profiles measured with an instrumented PackBot [2]. These scenarios represent typical tasks the robot is expected to perform during a mission. Various power profiles are combined in sequence to construct a "real-world" driving cycle from each of the shorter tasks.

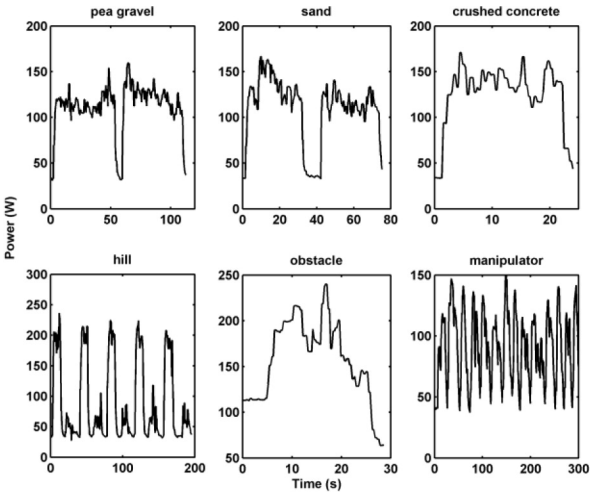

Figure 1. Power profiles sampled for typical terrain/operations at normal speed.

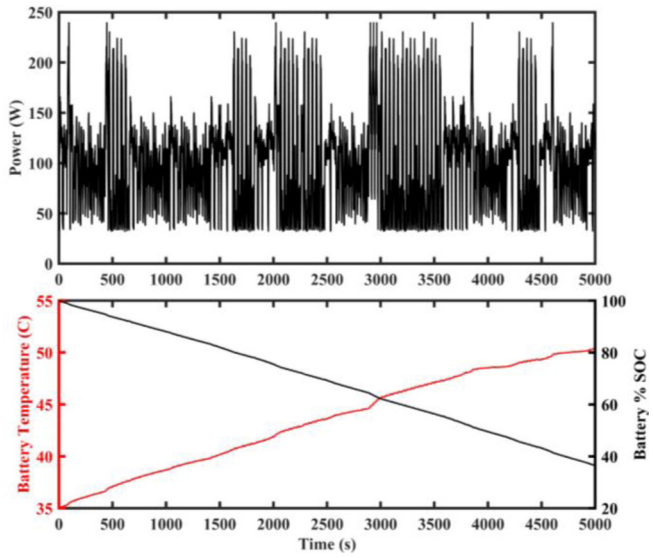

Figure 2. Synthetic power profile randomly generated by uniform sampling of the six mission profiles (top), and battery temperature (bottom) for case where robot is supported by only one BB2590.

As shown in Table 1 and Figure 1, load profiles are sampled for traversing typical terrains including pea gravel, sand, crushed concrete and operations such as climbing hill, travelling over an obstacle or using the manipulator. It should be noted that power profiles vary greatly even for identical terrain or operation, depending on vehicle speed, weight and environmental conditions. For a 10-hour mission, the cycle to cycle difference could also be significant due to varying mix of different scenarios. In order to evaluate system performance consistently, a Synthetic power profile is constructed. The measured power from six short duration task profiles are randomly sampled, assuming a uniform probability, and stacked to build longer mission profile as shown in Figure 2. For this 10 hour cycle, the average power draw is 98 W, the maximum power draw is 240 W and the standard deviation is 46 W.

ARCHITECTURE AND MODELS

There are two common options for hybridizing the fuel cell with a battery, either direct parallel connection of battery and fuel cell with a diode (to prevent back feeding current into the fuel cell), or use of DC/DC converter with the load either connected to the FC or battery as shown in Fig. 3. Other variations combining the above schemes may also be considered such as utilizing a small buck converter for optimum efficiency point operation with direct connection for high power (thus enabling operation with smaller DC/DC converter rating) [18], [20].

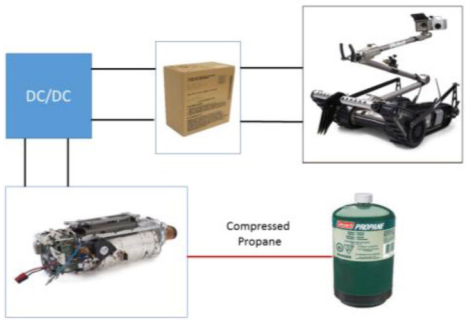

Figure 3. SOFC hybrid with DC/DC converter and high energy BB pack [2]

A DC/DC converter is connected between the battery and SOFC stack as shown in Fig. 3. Fuel cell auxiliaries are assumed to be powered by the battery pack to avoid issues of directly connecting unregulated loads to the fuel cell [19]. The SOFC is paired with a single low power high energy density BB-2590 pack because the SOFC can also provide high power, but has extended transitional phases (startup/shutdown) requiring significant energy to be provided from the battery.

Battery

The standard PackBot configuration uses 2 BB2590U packs storing 6.8 Ah each. Inside each ruggedized plastic container are 24 18650 cells packaged with electronics to perform battery management, protection, and cell balancing. The cells are connected 3 each in parallel and then 8 in series (3P8S) arrangement. Due to the packaging and sealed plastic waterproof container there is limited

heat rejection from the battery pack and temperature rise during operation is a concern for battery only operation [13], as shown by the 15 degree temperature rise in a few hours in Fig. 2.

The Battery pack can be modeled using a 4-state electro-thermal model of the cylindrical cell [15]. The model consists of two R-C equivalent circuits and state of charge (SOC) plus one thermal state. For the purpose of DP the battery model can be further reduced to 2 states (V_1 and SOC), when the battery temperature is well regulated, with little loss in fidelity. The reduced model consists of a single R-C equivalent circuit with series resistance and state of charge, appropriate for the low C-rate (<1C) operation of the battery [14]. The battery current is related to the battery power and load demand from the drive cycle by the following equation.

$$\begin{aligned} P_{batt} &= P_{dmd} + P_{aux} - P_{fc} \\ &= V_t\, I_{batt} = (V_{OCV}(SOC) - V_1 - I_{batt}R_{int})I_{batt} \end{aligned} \tag{1}$$

The open circuit voltage V_{OCV} is a function of the battery SOC, and the battery resistances R_1 and R_{int} depend strongly on temperature when cold, but remain relatively constant for the temperature range of interest here. The battery charging current is limited to 4.8A, with a manufacture recommended value of 3A. The charging current should be further reduced when the battery is near full charge such that the terminal voltage V_t does not exceed 33.6V. Therefore we limit the charging current to 3A during simulation of the hybrid system even if the FC is producing excess power.

$$\begin{aligned} I_{batt} &= \max(-3, I_{bc}) \\ I_{bc} &= \frac{(V_{OCV} - V_1) + \sqrt{(V_1 - V_{OCV})^2 - 4R_{int}(P_{dmd} + P_{aux} - P_{fc})}}{2R_{int}} \end{aligned} \tag{2}$$

The battery state of charge can be calculated from the battery current using the following equation

$$\frac{dSOC}{dt} = -\frac{I_{batt}}{Q_{cap}} \tag{3}$$

where Q_{cap} is the battery capacity. The voltage V_1 represents the capacitor voltage in the R-C branch of the equivalent circuit model.

$$\frac{dV_1}{dt} = \frac{I_{batt}}{C_1} - \frac{V_1}{C_1 R_1} \tag{4}$$

Finally the battery temperature, T_{batt}, is given by the following dynamic state equation,

$$m_{batt} C_p \frac{dT_{batt}}{dt} = h \cdot A \cdot (T_{batt} - T_{amb}) + Q_{gen}(P_{batt}, V_1, SOC) \ , \tag{5}$$

where m_{batt} and C_p are the battery mass and heat capacity. The convective heat transfer is proportional to the temperature difference between the battery and ambient air and $h \cdot A$ is the surface area times the heat transfer coefficient given in Table 2. Battery heat generation Q_{gen} is a combination of ohmic heat and entropic heat; the effects of enthalpy-of-mixing, phase-change, and heat capacity are neglected for simplicity [15].

Table 2. Battery model parameters

Parameter	Value (from [15])	Parameter	Value (from [22])
Q_{cap}	7.11, Ah	a	8.61e-6, 1/Ah-K^2
R_{int}	0.18, Ohm	b	-5.13e-3,1/Ah-K
A	5.76e-2, m^2	c	7.63e-1, 1/Ah
h	5, W/(m^2-K)	d	-6.7e-3, 1/K(C-rate)
m_{batt}	1.4, Kg	e	2.35, 1/(C-rate)
C_p	617, J/(Kg-K)	f	14876, 1/day$^{(1/2)}$
$V_{OCV}(0.2/0.8)$	29.68/31.86, V	E_a	24.5, KJ/mol
R_1	6.79E-2		
C_1	3246 Farads	T_{amb}	35^{o}C

To predict capacity fade of the battery, a semi-empirical model from [22] is adopted taking into consideration both calendar-life and cycle-life loss.

$$Q_{loss,\%} = Q_{loss,calendar} + Q_{loss,cycle} \tag{6}$$

Where, the cycle loss and calendar losses are given by,

$$Q_{loss,calendar} = ft^{0.5} \exp(-E_a / RT) \tag{7}$$

$$Q_{loss,cycle} = (aT_{batt}^2 + bT_{batt} + c)\exp((dT_{batt} + e)I_{rate})Ah_{throughput} \tag{8}$$

The former is modelled using a square root of time relation to account for the diffusion limited capacity loss and an Arrhenius correlation to capture the influence of temperature. The latter depends linearly on charge throughput while exponentially on current rate. The parameters of the capacity fade model and BB2590 electro-thermal model in Table 2 are experimentally derived in [22] and [16] respectively.

Solid Oxide Fuel Cell

The Ultra-AMI SOFC runs on readily available commercial propane cylinders, each containing about 0.5kg of propane. The fuel flow rate is pre-determined so as to maintain the delicate thermal balance within the stack and provide power for auxiliaries. Shutting down the fuel cell at low power demand is thus preferable to idling, because partial load operation is highly inefficient. However, the SOFC has an extended startup procedure requiring a significant amount of energy to heat up before power can be generated as explained in [1]. Similarly the shutdown procedure consumes battery energy to run the cooling fans. Therefore the SOFC must be paired with a relatively large energy storage battery (BB2590 pack).

However, as recently suggested by the manufacturer, it is possible to reduce fuel flow rate, and hence power generation rate, to some certain extent while keeping fuel efficiency unchanged at steady state. In other words, some partial load operating points can be made as efficient as full load. Multiple output power levels are thus introduced into the SOFC to study the improvement in fuel efficiency for the hybrid system.

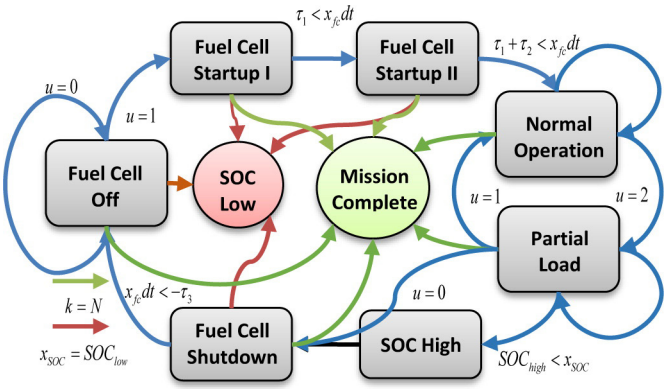

Figure 4. SOFC startup flow diagram [1].

The SOFC is modelled by four discrete phases, on and off, startup and shutdown, the latter two of which consume energy. The startup phase is further divided into two sub-phases, the second of which draw less electrical power than the first but consumes same rate of fuel as normal operation [1]. The on phase consists of several sub-phases, classified by their respective power levels and named as normal operation, partial load I, partial load II and so on. A flow chart showing how this hybrid system works is shown in Figure 4. The absorbing state Low SOC corresponds to depletion of the lithium ion battery when the FC is not on and hence mission failure.

Although we assume fuel efficiency is constant at steady state, even for part load operations, it is reduced during power level transition. A constraint ΔP needs to be imposed on rate of change in output power to avoid fuel depletion within stack [3], [8], [9]. The factor α is used to denote fraction of power wasted during FC power level transitions.

DYNAMIC PROGRAMMING FORMULATION

Dynamic programming is used to determine the optimal scheduling strategy that minimizes fuel consumption according to the following cost function [10],

$$\min_{u\in[0,1]} J = \sum_{k=1}^{N} W_{C_3H_8}(k) \tag{9}$$

where $W_{C_3H_8}$ is the fuel consumption rate (determined by assuming a constant fuel efficiency of 19% when on; and that startup phase II consumes same rate of fuel as normal operation). The state x_1 indicates the duration of time the fuel cell is in each transitional phase while x_2 denotes battery state of charge.

$$x_1(k) \in \left[-\frac{\tau_3}{dt}, \frac{\tau_1+\tau_2}{dt}\right]$$

$$x_1(k+1) = f(k) = \begin{cases} x_1(k)-1, -\tau_3 < x_1(k)dt < 0 \\ x_1(k)+1, 0 < x_1(k)dt < \tau_1+\tau_2 \\ 0, x_1(k) \le -\tau_3 \\ 0, x_1(k)=0, u(k)=0 \\ 1, x_1(k)=0, u(k)=1 \\ x_1(k), x_1(k)dt \ge \tau_1+\tau_2, u(k)=0 \\ -1, x_1(k)dt \ge \tau_1+\tau_2, u(k)=1 \end{cases} \tag{10}$$

$$x_2(k) = SOC(k) \in [SOC_{low}, SOC_{high}] \tag{11}$$

The control input $u(k)$ is a logical signal to initiate startup or shutdown with τ_1, τ_2 and τ_3 denoting durations of startup phase I/II and shutdown respectively. A 5s time step, dt, was applied for computation efficiency. The power profiles were averaged over the same time interval (8.5 hours) as shown in Figure 5.

Since the battery is operated at low C-rate (typically<1C) with a tightly controlled SOC, it is reasonable to remove V_1 from battery states to accelerate DP computation, especially for SOFC systems with multiple power levels. In the case where the battery upper voltage limit is a concern, such as constant current - constant voltage charging, the V_1 state should be included.

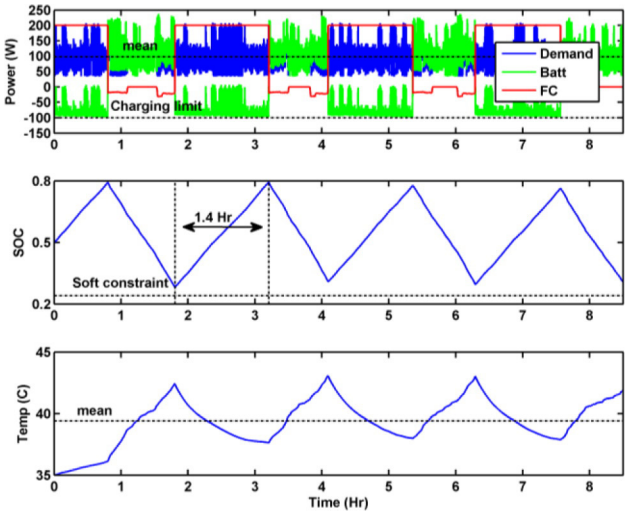

Figure 5. Simulation result for Synthetic power profile with fixed output

Initially the fuel cell is assumed to have a fixed output of 200W with no partial load power levels. Therefore it is most efficient to have the fuel cell fully loaded when on, and the control strategy is simply a series of on/off commands. The resulting SOC trajectory exhibits a cyclic and charge/discharge behavior as in Figure 5 rather than the classical monotonically decreasing one. Charge depletion is a natural result of fuel saving oriented DP because the optimal solution will always try to deplete energy stored in battery to save fuel for a given power profile [21]. Since the SOFC hybrid system uses only 1 BBPack, the temperature rise is an issue as shown in Figure 5. The average battery current during charging is lower than the discharging

portion of the cycle, when traction power is split between the battery and FC, causing the battery temperature to decrease. In addition, the entropic heating effect absorbs energy during charging for this specific battery chemistry.

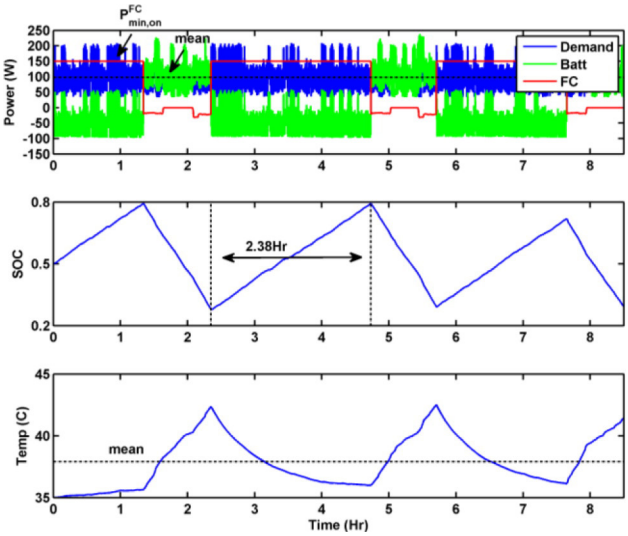

Figure 6. Simulation results for flexible output

The resulting efficiency is 14.0%, 26% lower than the nominal FC efficiency value of 19%. There are two major sources of energy loss, transitional phases (startup/shutdown) and the limited battery charging rate. Since batteries are used in a highly efficient way throughout the mission (C rate < 1C, and a tightly controlled SOC range), their losses due to internal resistance have limited impact on efficiency. Therefore, an intuitive solution to improve fuel efficiency is to reduce the number of FC shutdown/restarts and cut down on wasted/excess energy generation. The easiest way to achieve this goal is to decrease the operating power or reduce the size of the FC.

In comparison, consider a SOFC with flexible output power levels ranging from 150W to 300W so that average traction power can be better matched to the FC. Equation 13 shows the additional FC states denoting different power levels while Equation 14 shows added control command to transition to these states. The power is quantized with a unit of 10W, and therefore n equals 15 corresponding to the 150W range. A 10W/s constraint is imposed on rate of change in fuel cell output power by highly penalizing cases when $|x_1(k) - x_1(k-1)| > dt \;\forall\; x_1(k-1), x_1(k) > (\tau_1 + \tau_2) / dt$ [17]. The fuel consumption during startup phase II is normalized to 200W for consistency.

$$\min_{u\in[0,n]} J = \sum_{k=1}^{N} W_{C_3H_8}(k) \tag{12}$$

$$x_1(k) \in \left[-\frac{\tau_3}{dt}, \frac{\tau_1 + \tau_2 + ndt}{dt} \right] \tag{13}$$

$$x_1(k+1) = \{x_1(k) + u(k) - 1, x_1(k)dt >= \tau_1 + \tau_2, u(k) > 1\} \tag{14}$$

The SOC trajectory from flexible SOFC hybrid system, as shown in Figure 6, is similar to that of fixed output SOFC. The major difference from the previous results lies in the battery charging rate when fuel cell is on (150W instead of 200W). The battery pack is thus charged at a lower rate so that there will be fewer FC startups and shutdowns throughout the mission, greatly reducing the parasitic loss associated with these transitional phases. In addition, the wasted energy is greatly reduced as well, when FC output power minus traction power demand exceeds battery charging rate. With a lower charging rate the average battery temperature is also decreased (37.9 versus 39.4 degrees C), leading to a longer battery life. The resulting fuel efficiency is 16.4%, which is 17% higher than that of fixed output SOFC hybrid system, thanks to fewer transitional phases and less wasted energy from battery charging rate limits.

If the FC shutdown and restart cycle can be robustly avoided, then fuel efficiency would be greatly improved. The SOFC higher power level needs to be sized larger than average power demand to complete the mission. In that case, battery SOC will eventually reach the higher bound. At which point, if the SOFC is not shut down, it will operate at part load, which is very inefficient. Therefore, the lower power level should be set below the average mission demand to allow battery discharging without shutting down the SOFC. When power demand of the mission lies within that range, it is possible to avoid shutdowns throughout the mission, although the SOFC has limited load following capability due to the constraint on rate of power change and thermal management. Running DP for such a system shall generate a monotonically decreasing SOC trajectory, which is typical of charge depletion DP instead of cyclic behavior as shown below.

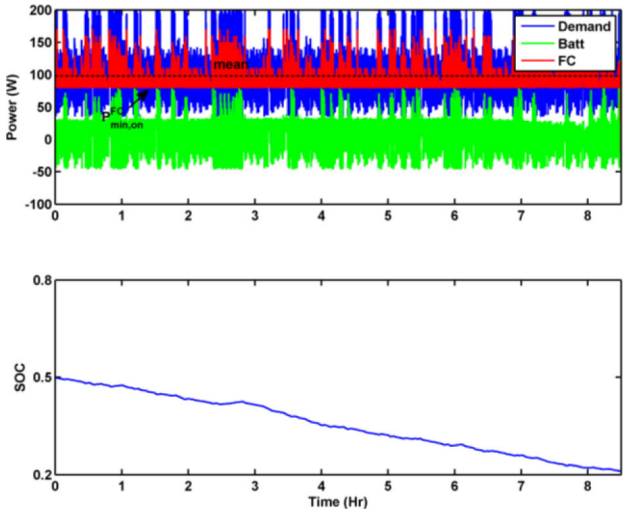

Figure 7. Simulation results for wider range output SOFC hybrid showing varying FC power levels can achieve a monotonically decreasing SOC trajectory.

When the power range of SOFC is extended from 80W to 300W with the same constraint on rate of change in FC output power. It is shown in Figure 7 that the SOFC works somewhere around average power demand throughout the mission while the battery is slowly discharged until it reaches lower SOC bound. The batteries are used in a moderate way with limited charge rate and temperature rise; 35.75 degrees C at the end of the cycle. These results agree with earlier analysis and it can thus be concluded that whether the fuel cell will experience cyclic startup/shutdown depends on overall power

demand level. When the average power demand of the cycle is well below FC power range, cyclic operation is inevitable, as is the case for stationary or creeping operation. On the contrary, when the average mission power lies within that range, the optimal strategy is to follow power demand with SOFC and try to fully discharge battery throughout the mission.

HYSTERETIC CONTROL WITH TWO POWER LEVELS

The efficiency achieved by SOFC hybrid system under optimal DP control with a wider power range is 18.9%, a value very close to the nominal FE of the FC alone when operated at constant power. However, in reality it is impossible to acquire cycle information in advance, and a rule-based controller needs to be constructed following the idea of optimal strategy from DP. A bang-bang controller can thus be built with four control parameters: p_l , p_h , SOC_{up} and SOC_{down}. The first two terms denote the higher and lower FC power generation levels. From results of DP it is clear that they should be set in a way such that the average power demand of the mission lies between them. The latter two terms denote battery SOC thresholds at which the FC should switch from the low to high power level and vice versa.

The performance of the bang-bang controller is simulated for various combinations of power level and SOC thresholds to evaluate the system efficiency. For a given pair of FC power levels, every possible SOC threshold combination is evaluated. For each pair of SOC thresholds three simulations are conducted with the battery SOC initialized to the quartiles of that range. After the fuel is depleted (each cylinder contains 500g of propane) the final battery states are recorded. The resulting fuel efficiency from the simulation is corrected for the difference between initial and final SOC. The energy required to restore the battery to its initial SOC following the way it is charged/discharged during the cycle, (at the same average C-rate) is used for the correction. Energy recuperated or dissipated during this process is then added to/subtracted from the energy of the propane fuel to estimate fuel efficiency. This is a little different from traditional SOC correction methods, because energy charged into the battery can only be partially recuperated in the way of discharging following the way it is used during the cycle. The same logic applies to cycles ending with low SOC by requiring charging back to the original level.

The interval between higher and lower SOFC power levels is initially set to be large so that the design is most robust as it can deal with all power demands lying within that interval. The lower SOC threshold is set no larger than 0.46 while the upper one no smaller than 0.54 so that power level transition will not be scheduled too often to induce stack degradation. The resulting efficiency is plotted in Figure 8 (bottom line denoted by circles).

Several comments can be made regarding the results. Firstly, for a given SOC interval, efficiency is insensitive to normal operating SOC, defined by (SOC_{up} + SOC_{down})/2, since the number of FC power transition remains constant. Additionally, the battery performance does not change within SOC range of investigation. Therefore efficiency can be plotted as a function of SOC interval instead of SOC threshold combination. Secondly, a larger SOC interval leads to fewer FC power level transition, but it does not necessarily guarantee a higher efficiency as in the case for fixed output SOFC hybrid system. Although fuel efficiency does suffer from power level transition, its impact is limited in contrast to FC startup/shutdown because it only lasts for around 10 seconds and is still providing power instead of drawing.

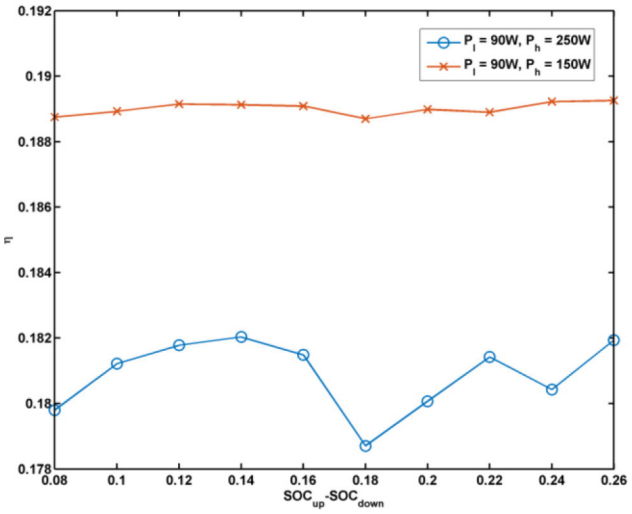

Figure 8. Fuel efficiency for P_l=90W, P_h =250W (bottom) and P_l=90W, P_h =150W (top) with varying SOC intervals with normal SOC = 0.5.

Fuel efficiency achieved with this pair of power levels is around 18.1%, smaller than the nominal value of 19% as shown in Table 3. Given that the battery charge rate is limited to 3A by the manufacturer's specification, if the higher FC power level is set too large, then fuel cell generated power (minus the energy used by the robot) in excess of the maximum battery charging rate is effectively wasted.

Reducing the upper FC power level by 100W results in improvement in FE. As shown in Figure 8 (top line), efficiency still varies with SOC threshold interval but the amplitude is limited compared to the original pair of power levels. FC startup and shutdown cycling is avoided. Most SOC intervals achieve a fuel efficiency no smaller than 18.9%, showing that for well-chosen power levels the impact of SOC threshold variation is greatly mitigated. The average battery capacity fade is slightly larger than that obtained with original FC powers levels. This seems a little counter intuitive because with a tighter power level interval, the battery has lower Ah throughput due to fewer charge discharge cycles and therefore a smaller $Q_{loss,cycle}$. In this case, cutting down energy loss from limited battery charging rate leads to a significant improvement in fuel efficiency and therefore a longer runtime. However, the capacity degradation is dominated by time (calendar loss), and therefore the longer runtime from higher FE leads to more battery degradation over the cycle.

The FE and battery capacity fade for several FC power levels were compared and listed in Table 3. The 105/90W limits are superior to any other combination in terms of both fuel efficiency and battery capacity fade because batteries are operated at the lowest battery C-rate, with which the number of FC power level transition and energy loss from battery internal resistance will be limited. When one FC power level is set near the average power demand (98W), the fuel efficiency will be kept at a satisfactorily high level while battery capacity fade at a reasonably low level. The only exception of 250/90W as explained above. Figure 9 and 10 show the power split and SOC trajectory and resulting battery temperature for the 250/90W and 105/90W power levels respectively. The gentler battery charging rate in the case for P_h=105W can be seen in Fig 10, by the lower average battery temperature and longer charging duration. When the power level is near the average, the battery will most often operate with a low C-rate, improving overall system performance. One surprising fact is how quickly system performance degrades as FC power levels are moved away from average power demand (150/70W in contrast to 150/90W).

Table 3. Fuel efficiency and battery capacity fade for different pairs of FC power levels

FC power levels	Simulated FE (%)	P_{Rloss}/P_{trans} (W)	Expected FE (%)	Battery capacity fade Q_{loss} (%)	$Q_{loss,\ cycle}$ (%)
250/90	18.1	0.65/0.05	0.189	0.7945	0.0379
150/90	18.9	0.48/0.01	0.189	0.8056	0.0327
105/90	19.0	0.41/0.00	0.189	0.7980	0.0241
150/70	18.7	0.68/0.04	0.189	0.8244	0.0572
105/70	19.0	0.44/0.00	0.189	0.8104	0.0347

EFFICIENCY PREDICTION

A statistical model of the load demand profile can be used to predict the overall system efficiency as a function of the control parameters, p_l, p_h, SOC_{up} and SOC_{down}.

We assume that power demand is normally distributed, with an average p_0 and a standard deviation σ for a given cycle.

$$f(P=x)=\frac{1}{\sqrt{2\pi}\sigma}e^{-\frac{(x-P_0)^2}{2\sigma^2}} \tag{15}$$

Since V_{OCV} and R_{int} remain relatively constant over battery SOC and temperature ranges of interest, the average battery current when the FC is operating at the lower/higher power levels can be expressed as follows,

$$I_l=\frac{P-P_l}{V_{OCV}} \quad \text{and} \quad I_h=\frac{P-P_h}{V_{OCV}} \tag{16}$$

$$\overline{I}_l=E[I_l]=E\left[\frac{P-P_l}{V_{OCV}}\right]=\frac{P_0-P_l}{V_{OCV}} \tag{17}$$

$$\overline{I}_h=\frac{P_0-P_h}{V_{OCV}} \tag{18}$$

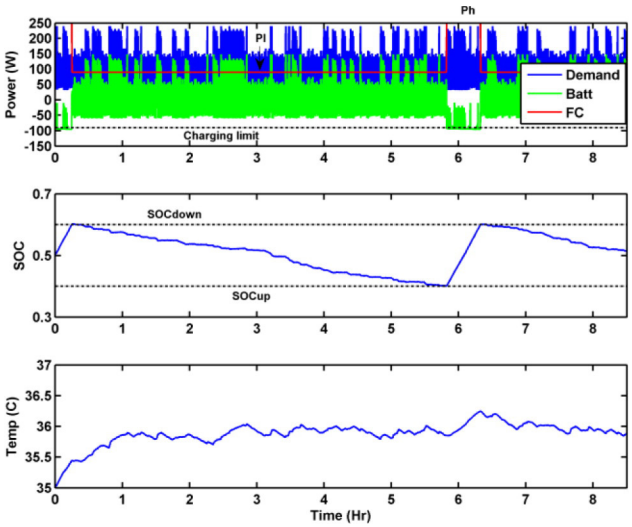

Figure 9. Mixed power profile for FC power levels (250/90W) showing power split, battery SOC and battery temperature.

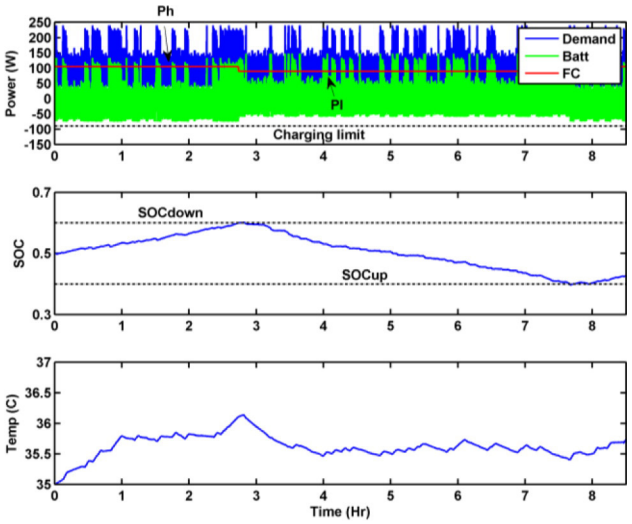

Figure 10. Simulation results for FC power levels (105/90W) showing slower battery charging rate and lower battery temperature compared to Fig 9.

To get a more general picture of fuel efficiency, assume it is evaluated over an infinite time horizon. The ratio of FC operating time at each of the two power levels can then be approximated as follows,

$$\tau=\frac{t_h}{t_l}=\frac{\frac{Q_{cap}(SOC_{down}-SOC_{up})}{-\overline{I}_h}}{\frac{Q_{cap}(SOC_{down}-SOC_{up})}{\overline{I}_l}}=\frac{P_0-P_l}{P_h-P_0}, \tag{19}$$

where t_h and t_l denote FC operation duration at each power level between two consecutive power level transitions. The average power loss due to battery internal resistance can be estimated as,

$$P_{Rloss} = E[I_h^2]R_{int}\frac{\tau}{\tau+1} + E[I_l^2]R_{int}\frac{1}{\tau+1}$$
$$= (E^2[I_h] + \mathrm{var}(I_h))\frac{R_{int}\tau}{\tau+1} + (E^2[I_l] + \mathrm{var}(I_l))\frac{R_{int}}{\tau+1}$$
$$= \left(\frac{(P_0-P_h)^2+\sigma^2}{V_{OCV}^2}\right)\frac{R_{int}\tau}{\tau+1} + \left(\frac{(P_0-P_l)^2+\sigma^2}{V_{OCV}^2}\right)\frac{R_{int}}{\tau+1}$$
$$= \frac{(P_0-P_l)(P_h-P_0)+\sigma^2}{V_{OCV}^2}R_{int} \quad (20)$$

Power loss associated with FC power level transition can be derived similarly,

$$P_{trans} = \frac{\alpha\frac{P_h+P_l}{2}\frac{P_h-P_l}{\Delta P}}{\frac{t_h+t_l}{2}} = \frac{\alpha(P_0-P_l)(P_h-P_0)(P_h+P_l)}{\Delta P Q_{cap}(SOC_{down}-SOC_{up})V_{OCV}} \quad (21)$$

where ΔP is the constraint on rate of change in FC output power (10W/s) and α is fraction of wasted fuel during power level transition, assumed here to be 0.2. Although the synthetic cycle is not normally distributed, performance is evaluated using power levels from Table 3. When power levels are moved away from average power demand, for example from 150/90W to 150/70W, P_{Rloss} and P_{trans} increase from 0.48/0.01W to 0.68/0.04W according to Equation 19 and 20, resulting in a noticeable decrease in efficiency. The expected fuel efficiency can be calculated using the following equation,

$$E[\eta] = 0.19\frac{P_0 - P_{Rloss} - P_{trans}}{P_0} \quad (22)$$

As shown by Equation 20, fuel efficiency benefits from a large SOC threshold interval as it is inversely proportional to P_{trans}. However, P_{trans} is orders of magnitude smaller than P_{Rloss} when FC power levels are chosen appropriately, suggesting choice of SOC thresholds has a limited impact on fuel efficiency, as is demonstrated by Figure 8 as well. Note that equations 16, 17, 18, 19, 20, 21, 22 are valid only when Ph is chosen such that the battery charging rate is not limited. Therefore for power levels (250/90W, 150/70W) the expected efficiency values from Equation 22 deviate from the results from simulation as shown in Table 2.

Selection of Power Levels

The dominant factor for determining fuel efficiency is selection of FC power levels. Design robustness is defined as the ability to avoid FC startup/shutdown or mission failure. A wider interval has the strongest robustness but is inferior to tighter intervals in terms of fuel efficiency and battery capacity fade. On the contrary, tighter interval achieves a fuel efficiency close to the nominal value but may be unable to avoid FC shutdown if there is an error in estimate of the average power demand. If the lower power level is chosen above the average power demand, the fuel cell will inevitably experience shutdowns and restarts, leading to a sharp drop in efficiency. The worst case takes place when the high power level falls below the average power demand of the cycle. In this case, the robot will fail the mission when the battery is depleted, being unable to get restarted without external help.

For the synthetic profile used in this study, the histogram of its power demand and the Gaussian fit are shown in Figure 11 with an average power of P_0=98 W. Based on Equations 16, 17, 18, 19, 20, 21, 22 the following heuristic can be used to choose the best power limits for the bang-bang controller.

1. Choose $P_h > P_0$ such that $Pr[I_h > -3A] \sim Pr[P > P_h - 3A*V_{ocv}]$ is sufficiently large (99%) to avoid battery charging rate limits. In this case, Ph can be any values between 98W and 123W and is set to 100W for initial guess.

2. Check if desired system performance is achieved. If not, then increase P_h as necessary for better robustness. As shown in Fig 12, decrease in fuel efficiency is limited compared to improvement in robustness as P_h is increased from 100W to 120W. Therefore P_h should be increased to 120W.

3. With P_h set, choose a P_l that balances FE and robustness to uncertainty in average mission power requirement. Choose P_l equal to 74W so that a robustness margin of 24W (from 98W) is obtained without sacrificing efficiency as shown in Fig 12.

4. Verify the selected FC power levels using the simulation models and repeat steps 2 and 3 if the results are unsatisfactory. Simulation results show that an efficiency as high as 18.97% is achieved and these power levels would be the final design.

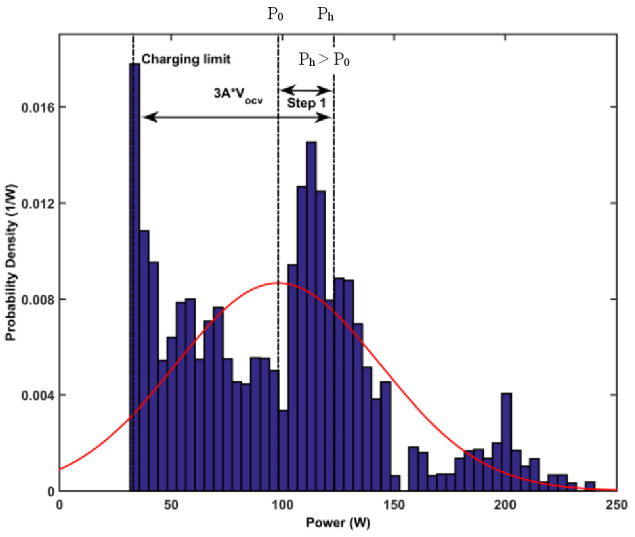

Figure 11. Histogram of the synthetic power profile and Gaussian fit used for predicting the system efficiency.

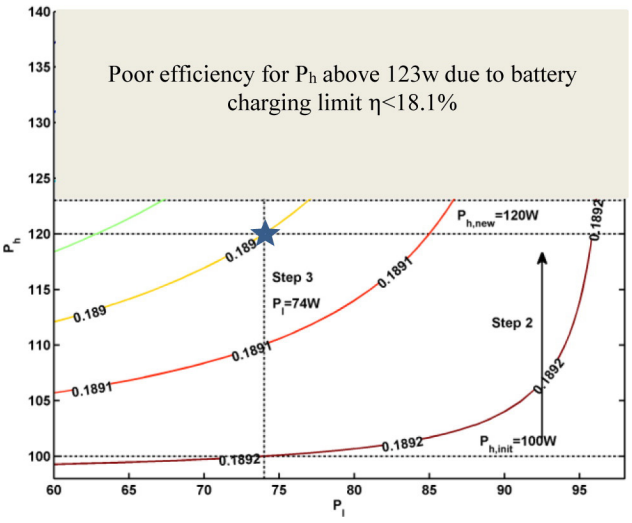

Figure 12. Expected fuel efficiency for different upper and lower FC power levels based on equation 21. Above 123W FC output power, the 3A battery charging limit may be active and therefore FE could be significantly lower than calculated by Eq 21.

CONCLUSIONS

In this paper, control strategies for a SOFC hybrid system with quantized power levels and large startup/shutdown penalties are investigated via Dynamic Programming and simulation models. It is shown that system performance is enhanced when the FC is able to produce multiple power levels instead of a single fixed one. Moreover, when the average power demand of the cycle lies within FC power range, it is possible to avoid transitional phases (startup/shutdown) throughout the mission and achieve a fuel efficiency close to nominal value.

It is further shown that near optimal system performance can be accomplished with a bang-bang controlled SOFC with only two power levels as long as average power demand is contained within and the battery capacity is sufficiently large. Different SOC threshold combinations are simulated with different FC power levels, showing that the former has a limited impact on system efficiency and the dominant factor for efficiency is selection of FC power levels. One major concern about selecting FC power levels is the tradeoff among design robustness, fuel efficiency and battery aging. A wider FC power interval excels in robustness but is inferior to tighter interval in terms of fuel efficiency and battery aging. Equations are then derived assuming power demand is normally distributed to quantify the tradeoff. Finally, general instructions about how to construct a rule-based controller for quantized power plant with large transitional loss is given and performed on the SOFC hybrid mobile robot based on distribution power demand.

REFERENCES

1. Broderick, John, Hartner Jack, Tilbury Dawn, and Atkins Ella. "Modeling and simulation of an unmanned ground vehicle power system." In SPIE Defense+ Security, pp. 908406-908406. International Society for Optics and Photonics, 2014.
2. Boice K., Leo A., Lee J., Paulson J. Jr., Skalny M., and Valascho T., "Baseline field testing of BB-2590 lithium-ion batteries using an iRobot Fastac 510 robot," tech. rep., TARDEC, 2010.
3. Mueller, Fabian, Jabbari Faryar, Gaynor Robert, and Brouwer Jacob. "Novel solid oxide fuel cell system for rapid load following." Journal of Power Sources 172, no.1 (2007): 308-323.
4. Liu J. and Peng H., "Modeling and Control of a Power-Split Hybrid Vehicle," IEEE Transactions on Control Systems Technology, vol. 16, no. 6, pp.1242-1251, 2008
5. Lin C.C., Peng H., Grizzle J. W., and Kang J., "Power Management Strategy for a Parallel Hybrid Electric Truck," IEEE Transactions on Control Systems Technology, vol. 11, pp. 839-849, November 2003
6. Guzzella L. and Sciarretta A., "Vehicle Propulsion Systems -Introduction to Modeling and Optimization", 3rd. Ed., 2013, Springer
7. Pukrushpan J. T., Stefanopoulou A. G., and Peng H., "Control of Fuel Cell Power Systems - Principles, Modeling, Analysis and Feedback Design," 2004, Springer
8. Vahidi A., Stefanopoulou A. G., and Peng H., "Current Management in a Hybrid Fuel Cell Power System: A Model Predictive Control approach," IEEE Transactions on Control Systems Technology, vol. 14, pp. 1047-1057, 2006
9. Vahidi A., Kolmanovsky I., and Stefanopoulou A. G., "Constraint Handling in a Fuel Cell System: A Fast Reference Governor Approach," IEEE Transactions on Control Systems Technology, vol. 15, pp. 86-98, 2007
10. Sundstrom O. and Stefanopoulou A. G., "Optimal power split in fuel cell hybrid electric vehicle with different battery sizes, drive cycles, and objectives," In Proc. IEEE Computer Aided Control System Design IEEE International Conference on Control Applications IEEE International Symposium on Intelligent Control, pp. 1681-1688, 4-6 Oct. 2006
11. Tsourapas V., Sun J., and Stefanopoulou A., "Control oriented analysis of a hybrid solid oxide fuel cell and gas turbine system," Journal of Fuel Cell Science and Technology, vol. 6, no. 4, 041008, 2009
12. Oh S.R., Sun J., Dobbs H., and King J., "Model Predictive Control for Power and Thermal Management of an Integrated Solid Oxide Fuel Cell and Turbocharger System," IEEE Transactions on Control Systems Technology, vol.22, no.3, pp.911-920, 2014
13. Ersal T., Kim Y., Broderick J., Guo T., Sadrpour A., Stefanopoulou A., Siegel J. B., Tilbury D., Atkins E., Peng H., Jin J. and Ulsoy A. G., "Keeping ground robots on the move through battery and mission management," ASME Dynamic Systems and Control Magazine, vol. 2, no. 2, pp. 1-6, 2014
14. Li Y., and Anderson D.. "Estimation and Compensation of Battery Measurement and Asynchronous Biases". US Patent Application no 2015/0158395.
15. Lin X., Perez H. E., Mohan S., Siegel J. B., Stefanopoulou A. G., Ding Y. and Castanier Matthew P.. "A Lumped-Parameter Electro-thermal Model for Cylindrical Batteries", Vol. 257, pp. 1-11, Journal of Power Sources, 2014.
16. Kim Y., Mohan S., Siegel J.B., Stefanopoulou A.G., and Ding Y, "The Estimation of Temperature Distribution in Cylindrical Battery Cells under Unknown Cooling Conditions", IEEE Transactions on Control Systems Technology.
17. Sundstrom O., Stefanopoulou A. G., "Optimum Battery Size for Fuel Cell Hybrid Electric Vehicle, Part I," ASME Journal of Fuel Cell Science and Technology, vol. 4, pp. 167-175, May 2007.
18. Nishizawa Akira, Kallo Josef, Garrot Olivier, Weiss-Ungethüm Jörg, "Fuel cell and Li-ion battery direct hybridization system for aircraft applications," Journal of Power Sources, vol. 222, pp. 294-300, January 2013.
19. Suh K. and Stefanopoulou A. G.. "Performance Limitations of Air Flow Control in Power-Autonomous Fuel Cell Systems." IEEE Transactions on Control Systems Technology, vol. 15, no. 3, pp. 465-473, May 2007
20. Lai Jih-Sheng; Nelson, D.J., "Energy management power converters in hybrid electric and fuel cell vehicles," Proceedings of the IEEE, vol.95, no.4, pp.766-777, April 2007.
21. Bubna, Piyush, et al. "Prediction-based optimal power management in a fuel cell/battery plug-in hybrid vehicle." Journal of Power Sources 195.19 (2010): 6699-6708.
22. Wang, John, et al. "Degradation of lithium ion batteries employing graphite negatives and nickel-cobalt-manganese oxide+ spinel manganese oxide positives: Part 1, aging mechanisms and life estimation." Journal of Power Sources 269 (2014): 937-948.

CONTACT INFORMATION

The authors may be contacted by
siegeljb@umich.edu
yuanzwan@umich.edu

DISCLAIMER

Reference herein to any specific commercial company, product, process, or service by trade name, trademark, manufacturer, or otherwise, does not necessarily constitute or imply its endorsement, recommendation, or favoring by the United States Government or the Department of the Army (DoA). The opinions of the authors expressed herein do not necessarily state or reflect those of the United States Government or the DoA, and shall not be used for advertising or product endorsement purposes.
UNCLASSIFIED: Distribution Statement A.

ACKNOWLEDGMENTS

The authors would like to acknowledge support from Kevin Centeck, Jack Hartner, and Denise Rizzo from the US Army TARDEC for their insight and advice about the mobile robot application and data from representative power profiles. The authors would also like to thank Tom Westrich from Ultra-USSI for insights about the SOFC system. Finally, the authors acknowledge the technical and financial support of the Automotive Research Center (ARC) in accordance with Cooperative Agreement W56HZV-14-2-0001 U.S. Army Tank Automotive Research, Development and Engineering Center (TARDEC) in Warren, MI.

DEFINITIONS/ABBREVIATIONS

SOFC - Solid oxide fuel cell

FE - Fuel efficiency

SOC - Battery state of charge

DP - Dynamic Programming

η - Efficiency

E[] - Expectation

Pr[] - Probability